# Deactivation Kinetics during Nanocarbonaceous Materials Production by CCVD.

*A. Monzón*, N. Latorre and T. Ubieto, A. Valera, E Romeo, C. Royo, J. I. Villacampa.*

*Department of Chemical and Environmental Engineering. University of Zaragoza. 50009 Zaragoza. Spain. E-mail: amonzon@unizar.es*

## INTRODUCTION.

The catalytic decomposition of hydrocarbons (e.g. methane or acetylene) over transition metals (Ni, Fe and Co) catalysts, also called Catalytic Chemical Vapour Deposition, CCVD, has recently been receiving attention as an alternative route to the production of hydrogen and nanocarbonaceous materials (NCM) from natural gas and other hydrocarbons [1-6]. Hydrogen is predicted to become a major source of energy in the future [7].

Hydrogen is a clean fuel that emits no $CO_2$ when burned or used in $H_2$-$O_2$ fuel cells, can be stored as a liquid or gas, is distributed via pipelines, and has been described as a long-term replacement for natural gas [7]. Therefore, a growing demand is forecast in all sectors, including petroleum refining where the increasing need to process heavy and high-sulphur content crude-oil is accompanied with the lowering of hydrogen co-product in the catalytic reforming process.

Steam reforming of methane and other hydrocarbon feedstocks has been the most widely used and usually the most economical technology for the production of hydrogen [7,8]. However, this route makes hydrogen an indirect source of $CO_2$. In addition, the co-product of steam reforming, CO, must be removed by two subsequent steps: water-gas shift and methanation. The complete removal of CO is not economical and therefore, the hydrogen thus produced is not suitable for low-temperature fuel cells given that the catalyst is poisoned by CO [1,9].

One of the advantages of catalytic decomposition of hydrocarbons it that avoids direct formation of $CO_2$ and, therefore subsequent steps for CO removal are not needed. In addition to Hydrogen production, CCVD produces nanocarbonaceous materials, namely carbon nanotubes, CNT's, and carbon nanofibres, CNF's. In fact, CNF's have been known for a long time as a nuisance that often appears during catalytic conversion of carbon containing gases. The recent outburst of interest in the NCM originates from their potential for unique applications as well as their chemical similarity to fullerenes and carbon nanotubes [10]. These materials have potential utilization as gas (e.g. hydrogen) storage, polymer additives, and as catalyst supports.

The accumulation of carbon in form of CNT's and CNF's allows the catalyst to maintain its activity in some cases for an extended period of time. However, catalyst deactivation usually occurs through the formation of encapsulating carbon on the nickel particles. The mechanism of carbon filament formation resulting from the decomposition of hydrocarbons on catalyst metal particles has been extensively studied in the past but few kinetic studies, including all the stages, have been reported.

In the present paper we report the results of catalytic behavior of a commercial Ni-Al catalyst (Harsaw, Ni-3266) during the reaction of methane decomposition.

A complete kinetic study of the main operating variables if this reaction (temperature and gas composition), has been made. The influence has been studied of the operating temperature and feed composition on the carbon formation rate, methane conversion as well as hydrogen production. The experimental procedures followed are the same as the explained in references 4 to 6.

It is worth noting that most kinetic studies presented in the literature only consider the period of constant carbon formation rate. However, our experiments indicate that the rate of carbon formation is not constant and follows a quite complex pattern. For this reason, the evolution of the carbon formation rate over time, including catalyst deactivation, has been measured during the complete duration of each experiment.

## KINETIC MODEL OF NANOCARBONACOUS FILAMENTS GROWTH.

The mathematical description of the kinetic model takes into account all stages of carbon formation: nucleation, filament growth and also the deactivation of the catalyst. These stages are explained in the following paragraphs.

*A) Hydrocarbon decomposition over the catalytic surface and catalyst deactivation.*

This stage can be expressed through the following individual steps:

$$CH_4 + 2l \rightarrow CH_3 - l + H - l \qquad \text{(m1)}$$

$$CH_3 - l + l \Leftrightarrow CH_2 - l + H - l \qquad \text{(m2)}$$

$$CH_2 - l + l \Leftrightarrow CH - l + H - l \qquad \text{(m3)}$$

$$CH - l + l \Leftrightarrow C - l + H - l \qquad \text{(m4)}$$

$$2H - l \Leftrightarrow H_2 + 2l \qquad \text{(m5)}$$

After the hydrocarbon decomposition stage, atoms of carbon and gaseous hydrogen are released over the catalyst surface. It is assumed that the number of active sites involved in the controlling step (named as *m*) of the methane decomposition is *m=2* (11-13).

Step of reversible formation of encapsulating coke. This step goes through reactions of condensation-oligomerization:

$$hCH_x - l \Leftrightarrow Pl_h + H_2 \qquad \text{(m6)}$$

The number of active sites involved in the controlling of the coke formation is named as *h* (14-17).

*B) Formation of carbide surface over the active catalyst surface.*

The atoms of carbon react with the metal at the surface forming a superficial carbide. This carbide is unstable at the reaction conditions. After this decomposition-segregation step the carbon atoms are introduced inside the bulk metal particles (11-13). This step determines the value of the carbon concentration at the interphase carbide-cristallite.

This individual step can be expressed as:

$$n(C-l) \rightarrow nC_B + nl \qquad \text{(m7)}$$

Is assumed that the rate of formation of the surface carbide follows a first order law:

$$\frac{dC_B}{dt} = r_D \cdot (C_S \cdot a - C_B) \qquad (1)$$

$C_B$ represents the carbon concentration on the metallic particle surface at the side in contact with gas phase.

The term $r_D$ represents the net rate of methane decomposition over the metallic surface. The rate decomposition depends of the reaction conditions, $r_D = \varphi(p_{CH_4}, p_{H_2}, Temp.)$, and this dependence can be derived from the mechanism presented above (12,13).

The term $C_{S_0}$ express the maximum surface concentration of carbon that can be formed over the fresh catalyst (i.e. without deactivation). This carbon concentration depends of the total active surface exposed by the catalyst. Therefore, if the catalyst is deactivated by the formation of encapsulating coke and/or by sintering, the exposed metallic surface will be diminished.

If the deactivation is produced by deposition of encapsulating coke, this process can be partially reversible because the hydrogen present in the reaction atmosphere can react with the coke, regenerating part of the catalyst surface. This fact produces that the catalyst do not suffers a complete deactivation, reaching a residual level of activity, which also depends on the reaction temperature and atmosphere composition.

In these conditions, the deactivation kinetics can be expressed as: (14-17):

$$-\frac{da}{dt} = \psi_d \cdot a^d - \psi_r \cdot (a^{d_m} - a) \qquad (2)$$

The terms $\psi_d$ and $\psi_r$ are respectively the "*deactivation and regeneration kinetic functions"* and, both depends on the operating conditions, (14-17). In addition, the kinetic orders *d* and $d_m$ are expressed in function of *m* and *h* as:

$$d = \frac{m+h-1}{m} \quad ; \quad d_m = \frac{m-1}{m} \tag{3}$$

As was mentioned, *m* and *h* represent the number of active sited involved in the controlling steps of the main (methane decomposition) and of the deactivation (coke formation) reactions.

During the integration of equation 2, arise several type of mathematical solutions depending of the values of *m* and *h*. Taking into account the mechanism exposed above, equations m1 to m7, the values of 1 and 2 are taken as the most plausible for *m* and *h*.

The best fits of the experimental data are obtained for the case of *h=1*. In this case, the equation 2 can re-written as:

$$-\frac{da}{dt} = \psi_G \cdot a^{d_m} \cdot \left(a^{1/m} - a_S^{1/m}\right) \tag{4}$$

The term $a_S$ represents the residual activity of the catalyst. $a_S$ and $\psi_G$, depend of $\psi_d$ and $\psi_r$ according to the next expressions:

$$a_S = \left(\psi_r / \psi_G\right)^m \quad ; \quad \psi_G = \psi_d + \psi_r \tag{5}$$

The resolution of equation 4 allows obtaining the explicit dependence of the catalyst activity with the time:

$$a = \left( a_S^{1/m} + \left(1 - a_S^{1/m}\right) \cdot \exp\left( -\frac{\psi_G}{m} \cdot t \right) \right)^m \tag{6}$$

<u>*C) Carbon diffusion and formation of carbon nanofilaments (NCM)*</u>

This stage represents the bulk diffusion of atoms of carbon through the metallic crystallites. This diffusion process determines the rate of formation of carbon nanofilaments. The rate of this step can be expressed as:

$$r_C = k_C\left(C_B - C_F\right) \tag{7}$$

The term $k_C$ is the effective transport coefficient of carbon on the Ni particles and depends on the average size of the Ni crystallites, the metallic exposed area, and of the carbon diffusivity: $k_C \approx a_{Ni}(D_C / d_{Ni})$.

The term $C_F$ is the carbon concentration at the support side. This value is initially zero, and when the carbon concentration at this side reaches a value higher than the solubility of the nanofilaments on the metallic particles, begins the precipitation of the carbon nanofilaments. This step determines the nucleation stage.

Further on this point, the carbon concentration at the interphase metal-filament is constant and equal to the solubility of the carbon filaments. The thermodynamics properties of the filaments determine the value of $C_F$. After the nucleation step, during the growing of the filaments the interphase metal-support is substituted by an interphase metal-filament.

Assuming that the value of $C_F$ is very low compared to the value of $C_B$, the rate of carbon accumulation over the catalyst can be calculated as:

$$r_C \approx k_C \cdot C_B \tag{8}$$

Solving simultaneously, equations 1, 6 and 8, for the case of *m=1*, the rate of carbon formation can be calculated as:

$$r_C(t) = r_{C_0}\left[a_S + \psi_G \alpha_1 \exp(-\psi_G t) - r_D \alpha_2 \exp(-r_D t)\right] \tag{9}$$

The terms $\alpha_1$ and $\alpha_2$ are given by:

$$\alpha_1 = \frac{r_D(1-a_S)}{\psi_G(r_D-\psi_G)} \quad ; \quad \alpha_2 = \frac{(r_D-\psi_G a_S)}{r_D(r_D-\psi_G)} \tag{10}$$

The term $r_{C_0}$ express the rate of carbon formation reached at the steady state, in absence of catalyst deactivation. This rate is calculated as:

$$r_{C_0} = k_C \cdot C_{S_0} \tag{11}$$

Therefore, the residual rate of carbon formation can be calculated as:

$$r_{C_S} = r_C(t)\Big|_{t\to\infty} = r_{C_0} \cdot a_S \tag{12}$$

In the case that the catalyst does not suffer deactivation, $r_{C_0}$ and $r_{C_S}$ are equals. On the other hand, in the case that the catalyst will be completely deactivated, $r_{C_S}$ will be zero $(a_S = 0)$.

Finally, the amount of NCM accumulated over the catalyst in a given time can be calculated as:

$$m_C(t) = \int r_C(t)dt = k_C \int C_B(t)dt \tag{13}$$

Integrating the above expression, the following equation is deduced:

$$m_C(t) = r_{C_0}\left[a_S t + \alpha_1 \cdot (1 - \exp(-\psi_G t)) - \alpha_2 \cdot (1 - \exp(-r_D t))\right] \tag{14}$$

For the case that *m=2*, the equations obtained are:

$$r_C(t) = r_{C_0}\left[\begin{array}{l} a_S + k_G\alpha_1^* \exp(-k_G t) + \\ \dfrac{k_G\alpha_2^*}{2}\exp\left(-\dfrac{k_G}{2}t\right) - k_B\beta\exp(-k_B t)\end{array}\right] \tag{15}$$

$$m_C(t) = r_{C_0}\left[\begin{array}{l} a_S t + \alpha_1^*\left(1 - \exp(-k_G t)\right) + \\ \alpha_2^*\left(1 - \exp\left(-\dfrac{k_G}{2}t\right)\right) - \beta\left(1 - \exp(-k_B t)\right)\end{array}\right] \tag{16}$$

The terms $\alpha_1^*$ , $\alpha_2^*$ and $\beta$ are given by:

$$\alpha_1^* = \frac{k_B\left(1 - \sqrt{a_S}\right)^2}{k_G\left(k_B - k_G\right)} \tag{17a}$$

$$\alpha_2^* = \frac{8k_B\sqrt{a_S}\left(1 - \sqrt{a_S}\right)}{k_G\left(2k_B - k_G\right)} \tag{17b}$$

$$\beta = \frac{a_S}{k_B} + \frac{\left(1 - \sqrt{a_S}\right)^2}{\left(k_B - k_G\right)} + \frac{4\sqrt{a_S}\left(1 - \sqrt{a_S}\right)}{\left(2k_B - k_G\right)} \tag{17c}$$

The kinetic parameters of the model are $r_{C_0}$, $r_D$, $\psi_d$ and $\psi_r$. These parameters include the dependence of the reaction temperature (apparent activation energies) and atmosphere composition (partial kinetic orders), and of the type and composition of the catalyst used (exposed area and intrinsic reactivity).

In the case that the catalyst do no suffers deactivation is obtained that $\psi_d = \psi_r = 0$, $a_S = 1$, and the equations 9 and 14 (*m=1*) and 15 and 16 (*m=2*) are simplified to the same expressions:

$$r_C(t) = r_{C_0}\left(1 - \exp(-r_D t)\right) \tag{18}$$

$$m_C(t) = r_{C_0}\left[t - \frac{1}{r_D}(1 - \exp(-r_D t))\right] \tag{19}$$

The above kinetic model allows us to obtain explicit mathematical expressions of the dependence of carbon content, and hydrogen production, on time of reaction and reaction conditions. This expression can be used directly to fit the experimental data obtained in a thermobalance operated as a fixed bed differential reactor in order to obtain the kinetic parameters.

**EXPERIMENTAL RESULTS AND MODEL APLICATION.**

Figure1 show the effect of methane concentration on the rate of NCM formation and NCM content. The rate of NCM formation has been calculated from the numerical derivative of the experimental $C_{NCM}$ vs. time curves.

In Figure 1a it can be seen that the entire carbon formation rate curves, $r_C$, show an initial period of rapid growth until a maximum is reached, $r_{Cmax}$. This maximum is usually followed by a decrease in the carbon formation rate until a residual constant value is reached.

The initial period, immediately before the period of rapid carbon growth, is usually called the "*induction period*" [4,5, 11-13]. This induction period has been ascribed to a stage of filament nucleation and its extent depends on the operating conditions [11-13].

During the period of activity decay, the deactivation rate is higher than the rate of filament formation. The catalyst activity strongly diminishes until it reaches a residual activity.

It is noteworthy that, in the reaction of methane decomposition, the rate of carbon filament formation is, in fact, the reaction rate, and therefore a direct measurement of the true catalyst activity.

As mentioned above, in many cases, catalyst deactivation is caused by deposition of encapsulating coke through a secondary reaction. In this case, the higher the coking rate is, the higher is the deactivation rate and the lower is the remaining activity.

Figure 1b shows that the increase of $p_{CH_4}$ provokes an increase in the catalyst carbon content, an increase in the activation and deactivation rates and an increase in the maximum rate of carbon deposition, $r_{C_{max}}$ .

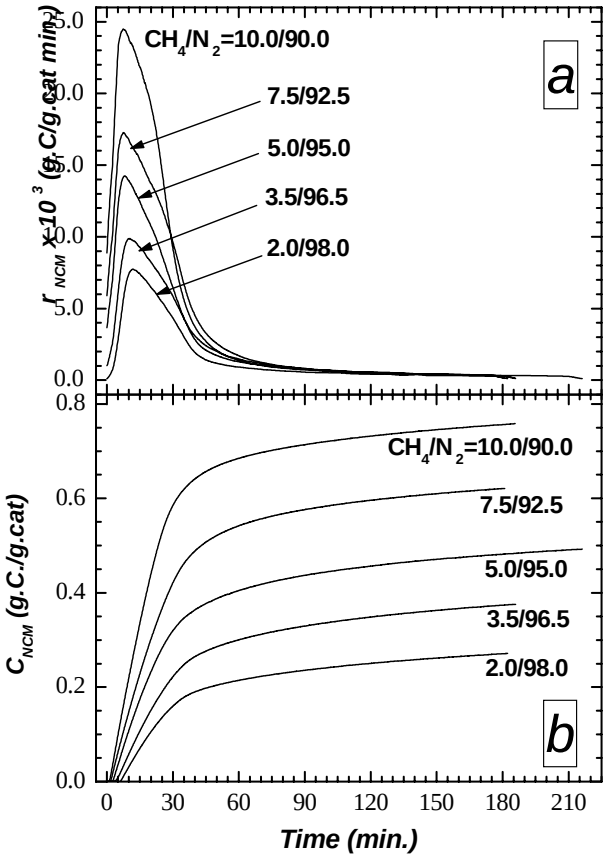


Figure 1. Evolution with time of $r_{NCM}$ (upper) and of $C_{NCM}$ (lower). Influence of $p_{CH4}$.

An increase in the methane concentration in the gas phase leads to a boost in the diffusion-precipitation process through the Ni crystallites. This in turn causes the increase in the initial reaction rate shown in Figure 1b. However, the greater the concentration of methane, the greater is the rate of formation of polymeric species which can encapsulate and deactivate the surface of the metallic crystallites [11-13]. This also explains the increase in the deactivation rate shown in Figure 1a.

The rest of the results obtained with the study of the other operating variables ( $p_{H_2}$ and temperature) can be analyzed in a similar mode.

In Figures 2a and 2b, are presented the results of the study of the influence of $p_{H_2}$ . In these figures is observed that an increase in $p_{H_2}$ causes a decrease in the carbon content on the catalyst, a decrease in the activation and deactivation rates and an increase in the residual rate of carbon formation. However, when the $p_{H_2}$ is varied from 0 to 0.04 atm., the effects are the opposite, leading to the presence of a maximum in the influence of $p_{H_2}$ over the carbon formation.

The position and magnitude of the maximum on $p_{H_2}$ effect, depends on the nature of the catalyst. The presence of this maximum can be explained by taking into account that, at low concentrations, the hydrogen prevents the formation of encapsulating coke, and consequently the formation of carbon filaments is not hindered by this coke.

However, at high $p_{H_2}$ the competition between $H_2$ and $CH_4$ for the active sites causes the diminution in the formation of both, carbon nanofilaments (negative effect) and encapsulating carbon species that deactivate the catalyst (positive effect). High hydrogen concentrations retard the formation of carbon filament but also prevent deactivation of the catalyst (Figure 2a). Under these conditions carbon formation rate is low (Figure 2b).

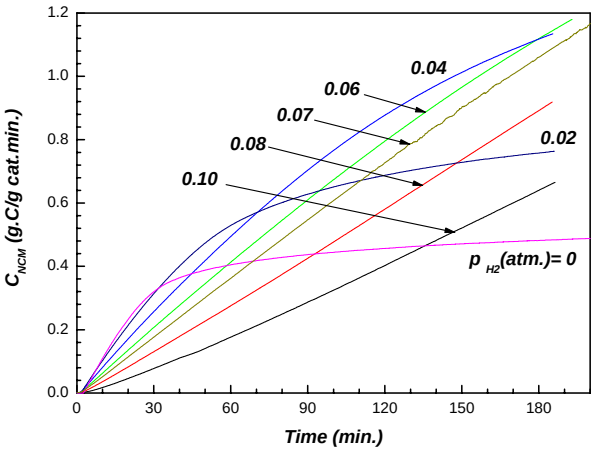


Figure 2a. Evolution with time of the of $C_{NCM}$. Influence of $p_{H2}$.

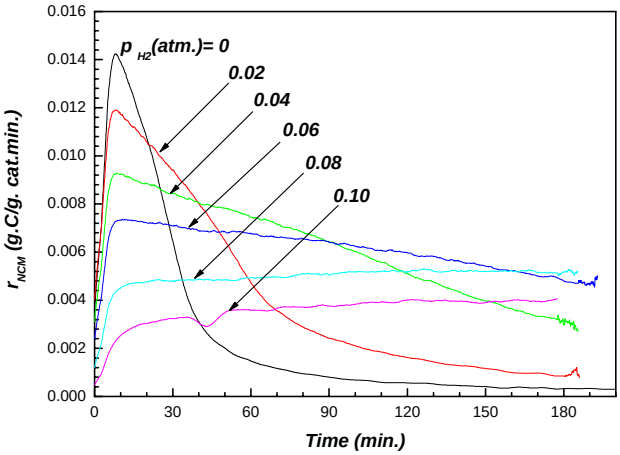


Figure 2b. Evolution with time of $r_{NCM}$. Influence of $p_{H2}$.

As regards the effect of the reaction temperature (results not shown) is obtained that, an increase in the reaction temperature causes a net decrease in the carbon content, but an increase in both the activation and the deactivation rates; as well as a slight decrease in the residual rate of carbon formation.

The fitting of the model has been done for both cases (*m=1* and *m=2*) and, although both fittings are very good, from a statistical point of view, the best results are obtained assuming *m=2* (i.e. equations 15 and 16). In addition, from the mechanism exposed above, is more straightforward assume a value of *m=2* in the decomposition of methane.

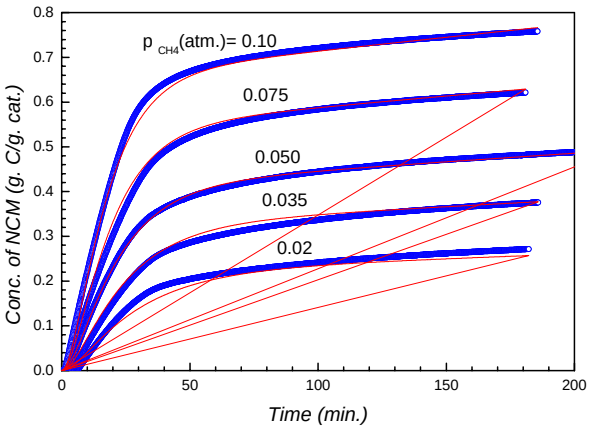


Figure 3. Model fitting to experimental data. Influence of $p_{CH4}$. *m=2*

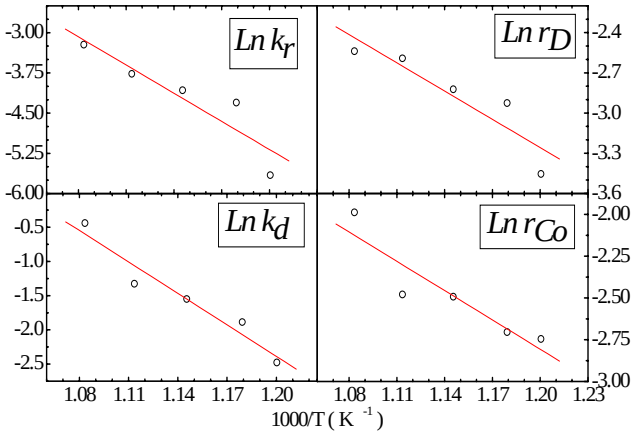


Figure 4. Arrhenius plots of the parameters of the model.

In Figure 3 is shown an example of the goodness of the fitting (carried out by non-linear multivariable regression) obtained with the developed model (eqn. 15).

The values of the kinetic parameters obtained in the studied of $p_{CH_4}$, $p_{H_2}$ and temperature, are presented in Tables 1, 2 and 3 respectively. As can bee seen, al the parameters presents very low values of the standard errors, indicating also a good fitting.

In Figure 4 are shown the *Arrhenius plots* of all the parameters of the model. The values of the apparent activation energies of the kinetic parameters are presented in table 4. These values of Ea are very similar to usual the values reported in the literature (5).

***Table 1. Kinetic parameters of NCM growth model. Influence of $p_{CH4}$.***

| $p_{CH4}$ (atm) | $k_r$±s.e. (x10$^2$) (min-1) | $k_d$±s.e. (x10$^2$) (min-1) | $r_D$±s.e. (x10$^2$) (min-1) | $r_{CO}$±s.e. (x10$^2$) (g NCM/g cat.min) |
|---|---|---|---|---|
| 0.100 | 1.012 ± 0.0050 | 10.91 ± 0.0880 | 13.21 ± 0.1290 | 6.99 ± 0.0550 |
| 0.075 | 1.012 ± 0.0050 | 8.29 ± 0.0550 | 12.62 ± 0.1170 | 4.24 ± 0.0270 |
| 0.050 | 1.012 ± 0.0050 | 7.02 ± 0.0410 | 16.49 ± 0.1770 | 2.71 ± 0.0150 |
| 0.035 | 1.012 ± 0.0050 | 6.08 ± 0.0390 | 13.21 ± 0.1590 | 1.80 ± 0.0110 |
| 0.020 | 1.012 ± 0.0050 | 6.09 ± 0.0520 | 11.98 ± 0.1900 | 1.30 ± 0.0110 |

***Table 2. Kinetic parameters of NCM growth model. Influence of $p_{H2}$.***

| $p_{H2}$ (atm) | $k_r$±s.e. (x10$^2$) (min$^{-1}$) | $k_d$±s.e. (x10$^1$) (min$^{-1}$) | $r_D$±s.e. (x10$^2$) (min$^{-1}$) | $r_{CO}$±s.e. (x10$^2$) (g MNCM/g cat.min) |
|---|---|---|---|---|
| 0 | 0.976 ± 0.005 | 6.79 ± 0.123 | 17.2 ± 1.3 | 2.64 ± 0.39 |
| 0.01 | 0.792 ±0.003 | 3.75 ± 0.106 | 24.8 ± 1.6 | 1.89 ± 0.53 |
| 0.02 | 0.451±0.004 | 2.53 ±0.097 | 21.9 ± 2.0 | 1.72 ± 0.12 |
| 0.03 | 0.398 ±0.01 | 1.30 ± 0.069 | 40.2 ± 2.9 | 1.24 ± 0.09 |
| 0.04 | 0 | 0.616 ± 0.021 | 32.3 ± 5.3 | 10.4 ± 0.08 |
| 0.06 | 0 | 0.232 ±0.016 | 44.6 ± 3.2 | 0.771 ± 0.002 |
| 0.07 | 0 | 0.111 ±0.011 | 35.1 ± 1.3 | 0.660 ± 0.008 |
| 0.08 | 0 | 0 | 19.3 ± 2.9 | 0.508 ± 0.009 |
| 0.10 | 0 | 0 | 7.4 ± 1.6 | 0.381 ± 0.010 |

***Table 3. Kinetic parameters of NCM growth model. Influence of Temperature.***

| Temp. $_{reaction}$ (ºC) | $k_r$±s.e. (x10$^2$) (min$^{-1}$) | $k_d$±s.e. (x10$^2$) (min$^{-1}$) | $r_D$±s.e. (x10$^2$) (min$^{-1}$) | $r_{CO}$±s.e. (x10$^2$) (g MNCM/g cat.min) |
|---|---|---|---|---|
| 560 | 0.35± 0.0270 | 8.40± 0.1480 | 3.16± 0.0510 | 6.42± 0.1420 |
| 575 | 1.35 ± 0.0050 | 15.17± 0.1340 | 5.36± 0.0300 | 6.69± 0.0640 |
| 600 | 1.70 ± 0.0080 | 21.26 ± 0.2560 | 5.94 ± 0.0350 | 8.27 ± 0.1050 |
| 625 | 2.31 ± 0.0180 | 26.52 ± 0.5380 | 7.49 ± 0.0730 | 8.38 ± 0.1780 |
| 650 | 3.98 ± 0.0630 | 64.44 ± 2.4250 | 7.89 ± 0.0720 | 13.71 ± 0.5330 |

***Table 4. Apparent activation energies of the parameters of the model.***

| | ***Ea ($k_r$)*** | ***Ea ($k_d$)*** | ***Ea ($r_D$)*** | ***Ea ($r_{Co}$)*** |
|---|---|---|---|---|
| ***$E_a$ (kJ/mol)*** | 145.5 ± 36.4 | 127.3 ± 18.6 | 58.4 ± 15.0 | 48.6 ± 11.9 |

These results clearly indicate that the proposed kinetic model also allows to separate and investigate the influence of each stage involved on the process of NCM growth, and therefore to have a more fundamental approach of this phenomenon.

**CONCLUSIONS.**

The direct catalytic cracking of methane over nickel catalysts is a potential alternative route for the production of NCM and hydrogen from natural gas. Ni catalysts are active for the methane cracking reaction at temperatures above 550 ºC.

The hydrogen competes with the methane for the Ni surface sites inhibiting both the formation of carbon filaments and the formation of encapsulating coke, which deactivates the catalyst.

An increase in the methane concentration leads to an increase in both the rate of carbon filament formation and the deactivation rate. The increase in methane concentration also increases the driving force for the filament formation, increasing both the number of filaments that can be formed and their nucleation rate. This effect intensifies at low $H_2$ concentrations in the feed, impeding the deactivation of the catalyst but without going so far as to inhibit filament formation.

An increase in the operating temperature favors the formation of both carbon filaments and encapsulating coke. At high reaction temperatures, the catalyst deactivation effect is more marked than that of the nucleation and growth of new filaments. This explains the reduction in the amount of carbon formed at high temperatures.

The kinetic model developed for carbon filament formation considers the stages of nucleation and the growth of the filaments. The kinetic parameters of the model ($r_{C0}$, $r_D$, $\psi_d$ and $\psi_r$) have been correlated satisfactorily with the main variables of the reaction: $p_{H_2}$, $p_{CH_2}$ and temperature.

In fact the proposed kinetic model also permit to separate and investigate the influence of each individual stage involved on the process of NCM growth, and therefore to have a more fundamental approach of this phenomenon.

**Acknowledgements.**

The authors acknowledge financial support from MEC, Madrid, Spain (Grant CTQ 2004-03973/PPQ).

**REFERENCES.**


1. N. Z. Muradov and T. N. Veziroglu; Int. J. Hydrogen Energy, **30** (2005) 225.
2. N. Z. Muradov; Int. J. Hydrogen Energy, **26** (2001) 1165.
3. T. Zhang and M.D. Amiridis; Appl. Catal. A, **167** (1998) 1161.
4. J.I. Villacampa, C. Royo, E. Romeo, J.A. Montoya, P. del Angel and A. Monzón; Appl. Catal. A, **252** (2003) 363–383.
5. M. Pérez-Cabero, E. Romeo, C. Royo, A. Monzón, A. Guerrero-Ruiz and I. Rodríguez-Ramos; J. Catal., **224**, (2004) 197.
6. De Chen, Kjersti O. Christensen, E. Ochoa-Fernández, Z. Yu, B, Tøtdal, N. Latorre, A. Monzón and A. Holmen; J. Catal., **229**, (2005) 82.
7. J.N. Armor, Appl. Catal. A; **176** (1999) 159.
8. J.M. Abrardo, V. Khurana; Hydrocarbon Proc., **79** (1995) 43.
9. M. Steinberg and H.C. Cheng; Int. J. Hydrogen Energy, 1**4** (1989) 797.
10. K.P. de Jong and J. W. Geus, Catal. Rev.–Sci and Eng., **42** (2000) 481.
11. I. Alstrup, I., J. Catal. 109 (1988) 241.
12. J.-W. Snoeck, G.F. Froment and M. Fowles; J. Catal., **169**, (1997) 240;
13. J.-W. Snoeck, G.F. Froment and M. Fowles; **169** (1997) 250.
14. J. Corella, J. Adanez and A. Monzón; Ind. Eng. Chem. Res., **27** (1988) 375-381.
15. A. Borgna, T.F. Garetto, A. Monzón and C.R. Apesteguía; J. Catal., **146** (1994) 69-81.
16. J.C. Rodriguez, J.A. Peña, A. Monzón, R. Hughes and K. Li; The Chem. Eng. J., **58** (1995) 7-13.
17. A. Monzón, E. Romeo and A. Borgna; Chem. Eng. J., **94** (2003) 19-28.